FEATURES OF THE PRESSURE DISTRIBUTION ON THE CONICAL TAIL PART

A.N. Kravtsov, V.Yu. Lunin, T.Yu. Melnichuk, A.V. Panyushkin
Central Aerohydrodynamic Institute named after prof. N.Ye. Zhukovsky (TsAGI)
140180 Zhukovsky, Moscow Region, Russia
Corresponding author: Tel.: +74955563542; E-mail: kravcow-an@rambler.ru

KEYWORDS:

Main subjects: flow visualization
Fluid: high speed flows, flows with shocks
Visualization method(s): numerical visualization
Other keywords: axisymmetric flow, conical stabilizer (flare), flare semiapex angle

ABSTRACT: The paper presents numerical research of the aerodynamic configuration with a conical tail part in the form of a truncated cone. Analysis of flow fields and space distributions of the gas-dynamic parameters was carried out. The calculated results and the experimental data are compared. The performed numerical visualization made it possible to elucidate the feature which is associated with the nonmonotonic character of the pressure distribution on the conical tail part.

Introduction. Different stabilizing and piloting devices are widely used on flying vehicles in order to achieve the desired stability. In some cases the stabilizing devices perform the role of control surfaces. In practical aerodynamics, wing-like surfaces and extending tail parts (conical stabilizers) are widely used as stabilizing devices. The effectiveness of a wing surface decreases with increasing free-stream Mach number and, at high Mach numbers, can become insufficient for stabilization of a rocket. In addition to that, at $M_\infty > 8$ wing stabilizers are subjected to aerodynamic heating and require thermal protection of their surface. In this regard it is reasonable to use conical stabilizers on particular types of flying vehicles. A conical stabilizer has a series of significant advantages. One is the fact that the value of the derivate of the normal force coefficient by the angle of attack C_y^α at supersonic speeds remains almost constant when Mach number M_∞ increases. Therefore, the effectiveness of the truncated cone shaped stabilizer does not change in a sufficiently large range of supersonic speeds.

The paper presents numerical research of the aerodynamic configuration which has a stabilizing device in the form of a truncated cone. The supersonic inviscid flow around the considered configuration was simulated using the Euler equations (Zhilin and Kovalenko[1]). The surface of the bow shock wave was treated explicitly. The Euler equations were integrated using the MacCormack finite-difference scheme. The viscid simulation results were obtained using the Reynolds-averaged Navier-Stokes equations.

Qualitative features of supersonic flow around a flying vehicle with a stabilizing device in the form of a truncated cone are considered. Characteristic feature is revealed which is associated with the nonmonotonic character of the pressure distribution on the flare. In order to study the revealed peculiarity, analysis of flow fields and space distributions of the gas-dynamic parameters in the flow and on the surface of the conical stabilizer was carried out, a numerical visualization was performed. Comparison of the numerical simulation results and the experimental data has been done.

1. Verification of the calculated results. Systematic experimental studies of models of blunted bodies of revolution with conical stabilizing devices were performed on SBT (small ballistic wind tunnel) at TsAGI (Krasil'shchikov and Gur'yashkin[2]). The test model was shot toward a supersonic flow at a velocity of 500 to 2000 m/s. The values of the Mach number of the flow M_f in the test section were M_f=2.5, 3.0, and 3.5. The resultant Mach numbers for the model shot toward the flow ranged within 6 – 14. To provide Mach numbers from 1.5 to 6, the test model was shot into the test chamber with the still air. For most tests in the ballistic wind tunnel, the Reynolds numbers Re varied from ~10^6 (at M_∞=1.5) to $20\cdot10^6$ (at M_∞=14).

In addition to measuring the drag of the flying vehicle with a stabilizing device in the form of a truncated cone, in Krasil'shchikov and Gur'yashkin[2] the flow fields near the models were investigated by means of the shadowgraph technique. One of the shadowgraphs (Glotov[3]) of flow around the blunted cylindrical body (M_∞ =3) with a conical stabilizer (a flare with a semiapex angle of θ =40°) obtained by Krasil'shchikov and Gur'yashkin[2] is shown in Fig. 1,a. In Krasil'shchikov and Gur'yashkin[2] it is noted that the studied models had a specific shape, in some cases the occurrence of boundary layer separation in front of the conical stabilizer could be expected. As a result of studying the experimental data an area of the development of the separated flow regions was determined, their length was measured, and the variation with Mach number was obtained. Fig 1,b shows the area of the existence of boundary layer separation depending on the free-stream Mach number and the conical stabilizer semiapex angle θ obtained from Krasil'shchikov and Gur'yashkin[2].

The results of numerical simulation of viscous supersonic flow around the considered sphere–cylinder–flare configurations in the framework of the Reynolds-averaged Navier-Stokes equations are shown in Figs. 1,c and 1,d. The flow pattern is presented for the experimentally visualized configuration of the flying vehicle with a conical stabilizer

semiapex angle of θ = 40° (M_∞ =3, Fig. 1,c) and the sphere–cylinder–flare configuration with a stabilizer semiapex angle of θ = 15° (M_∞ =3, Fig. 1,d). The structure of the shocks, expansion waves, and the vortex wake near the considered configurations is distinctly seen in Figs. 1,c and 1,d. Overlapping the results of numerical simulation of the flow pattern (Fig. 1,c) with the results of the experimental shadowgraph technique (Fig. 1,a), we obtain that the location of the bow shock wave, the shock wave determined by the conical stabilizer, and the point of their intersection are practically the same. The bow shock waves and the shock waves determined by the conical stabilizer after their intersection generate the strong shock front and the internal weaker shock. The calculated location of the resulting shocks also coincides with the results of the experimental visualization obtained in the ballistic laboratory (Figs. 1,a and 1,c).

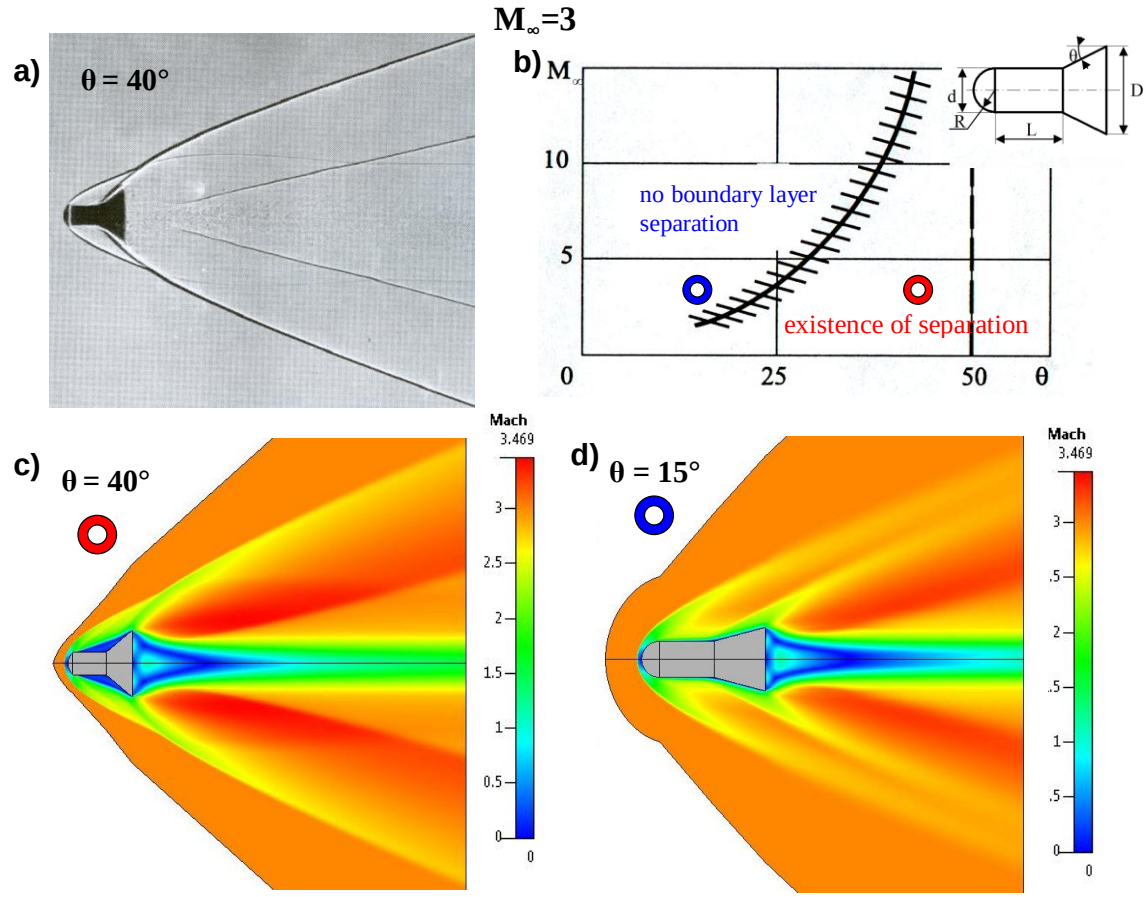

Fig. 1. Simulation of the flow field near the flying vehicle with a conical stabilizer (c, d – Mach contours)

The parameters of flow in the wake region of the considered configurations are characterized by an extreme complexity and highly differ from the values of the undisturbed flow. The recirculating region developing straight behind the base (the region of almost still air) and the region of attachment have the rectilinear boundaries. Behind the narrowest section (wake neck) the vortex wake stops narrowing and becomes almost cylindrical. In the region of the wake neck the wake neck wave appears with an almost conical front. The calculation results of the flow field in the region of the base (Fig. 1,c) including the recirculating region, the regions of attachment and recompression agree well with the experimental flow pattern (Fig. 1,a). The shapes of the vortex wake and the recirculating region are almost identical to those obtained in the experiment.

The diameter of the wake neck in the experiment is 20% smaller than in the calculation and is located downstream (10% of the total length of the model) The experimental value of the diameter of the vortex wake on the cylindrical portion exceeds the calculated value by about 25%. Meanwhile the calculated location of the wake neck shock (Fig. 1,c) in the recompression region coincided with the experimental result. (Fig. 1,a).

As is stated above the peculiarity of flow around the considered configurations is the existence of boundary layer separation in front of the conical stabilizer. Fig. 1,b shows that the sphere–cylinder–flare configuration (M_∞ =3, θ = 40°, Figs. 1,a and 1,c) according to the classification Krasil'shchikov and Gur'yashkin[2] falls within the area of the development of the separated region in front of the conical stabilizer. The results of numerical simulation as well as the experimental data prove the existence of separation with the development of the extensive recirculating region in front of the flare.

As a result of analyzing the experimental visualization of flow around the sphere–cylinder–flare configuration (Krasil'shchikov and Gur'yashkin[2]) it was found that boundary layer separation did not occur on the models with a

conical stabilizer semiapex angle of $\theta = 15°$ in the Mach number range of 2 to 14. The feature of the flow pattern around the sphere–cylinder–flare configuration ($M_\infty = 3$, $\theta = 15°$, Fig. 1,d) in accordance with the graph (Fig. 1,b) is flow without the development of the separated region in front of the conical stabilizer. As far as concerns the remaining structure of flow, it is qualitatively identical to that obtained for the sphere–cylinder–flare configuration with a conical stabilizer semiapex angle of $\theta = 40°$ ($M_\infty = 3$, Fig. 1,c).

2. Flow around the cone–cylinder–flare configuration. An example of numerical computation of aerodynamic loads on the surface of the cone–cylinder–flare configuration including the aft section of the configuration (the surface of the tail stabilizer) and a comparison with the results of experimental investigations (Coleman[4]) are presented in Fig. 2. The distribution of relative pressure P/P_∞ along the length of the cone-cylinder-flare configuration with a nose semiapex angle of $\delta \approx 10°$ (nose aspect ratio λ=2.9) and a conical stabilizer semiapex angle of $\theta = 30°$ at a free-stream Mach number of 9.22 is shown. The results of numerical simulation were obtained in the framework of the Euler equations and as the Reynolds-averaged Navier-Stokes equations. Behind the shock attached to the nose conical part the gas pressure increases approximately up to $5P_\infty$ and does not change along the whole length of the cone. At the joint of the conical nose and the cylindrical part flow expansion occurs, and the pressure on the cylindrical part becomes close to the static pressure of the undisturbed flow

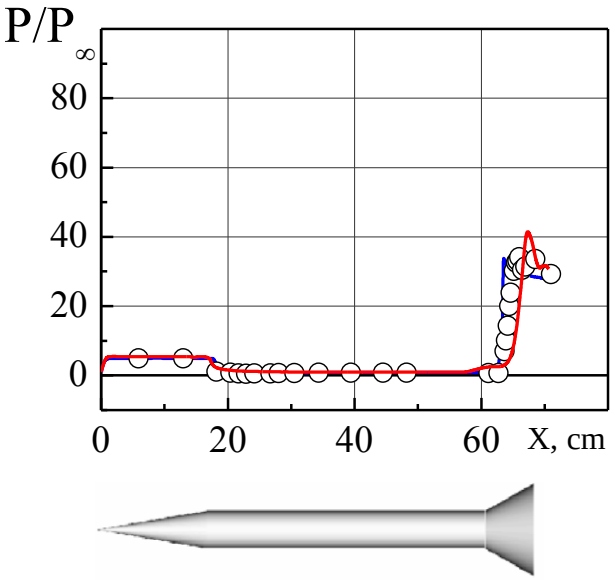

Fig. 2. Pressure distributions P/P_∞ on the cone-cylinder-flare configuration with a nose semiapex angle of $\delta \approx 10°$ and a conical stabilizer semiapex angle of $\theta = 30°$ at a free-stream Mach number of 9.22(○○○ – experiment (Coleman, 1973); calculation: —— – Euler, —— – Navier-Stokes)

($P/P_\infty \approx 0.9$). Up to the conical stabilizer the results of inviscid flow around the configuration with the stabilizing device agree well with the numerical simulation of the considered configuration carried out in the framework of the Reynolds averaged Navier-Stokes equations. The viscous flow results indicate the occurrence of separation in front of the flare. The calculations carried out in the frame of an ideal gas model do not take into account viscid effects (Fig. 2). On the surface of the flare the pressure abruptly increases achieving $P/P_\infty = 35 \div 28$ values. The highest pressure value is achieved at the beginning of the conical stabilizer, straight behind the shock attached to its surface.

Let's dwell on the pressure distributions on the surface of the flare in detail (Fig. 3). In the experiment in front of the flare a zone of boundary layer separation appears. The calculation in the framework of the Reynolds-averaged Navier-Stokes equations correctly defines the beginning of the pressure rise in the region of the conical stabilizer. The experimental data and the viscid solving results show the shock smearing appearing at the joint of the cylindrical part and the conical stabilizer. The viscid simulation results give farther location of the maximum in the pressure coefficient ($P/P_\infty = 42$) on the flare than the experimental data do. The experimental maximum value is $P/P_\infty = 36$. After reaching its maximum value the pressure decreases (Fig. 3). The experimental results show slight increase of pressure approximately in the region of the middle section of the stabilizer from $P/P_\infty = 32$ to 35. The calculations in the framework of the Reynolds averaged Navier-Stokes equations also indicate slight increase of pressure in the region of the middle section of the flare.

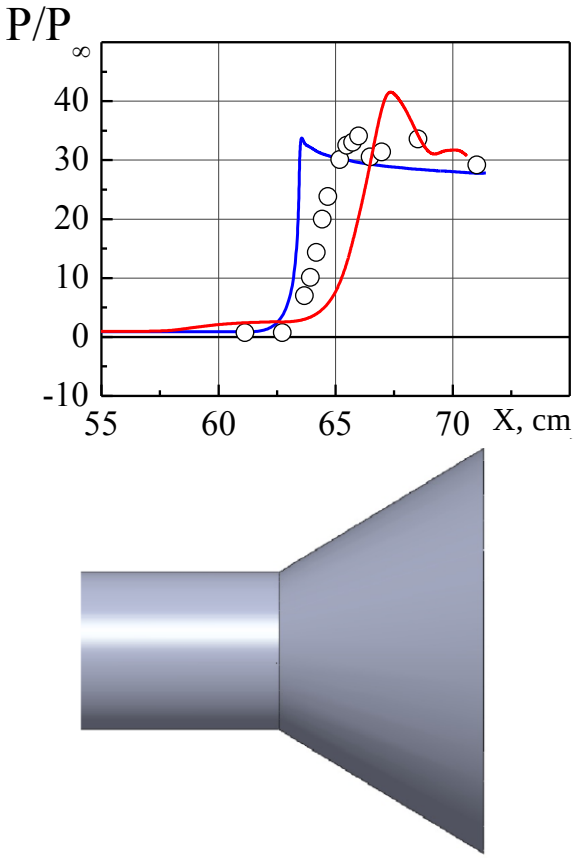

Fig. 3. Pressure distributions on the flare of the cone-cylinder-flare configuration at a free-stream Mach number of 9.22, the symbols are the same as shown in Fig. 2

3. Numerical visualization of flow around the conical stabilizer. The revealed peculiarity associated with the nonmonotonic character of the pressure distribution on the flare surface was numerically investigated for the cone-cylinder-flare configuration with a nose semiapex angle of $\delta \approx 35°$ (nose aspect ratio λ=0.7) and a conical stabilizer semiapex angle of $\theta = 35°$ at a free-stream Mach number of 7. This configuration has the smaller nose aspect ratio and the nonmonotonic character of the pressure distribution on the flare is shown more emphatically. The flow field structure in the longitudinal section of the cone-cylinder-flare configuration obtained as a result of numerical simulation of inviscid supersonic flow in the framework of the Euler equations is illustrated in Fig. 4.

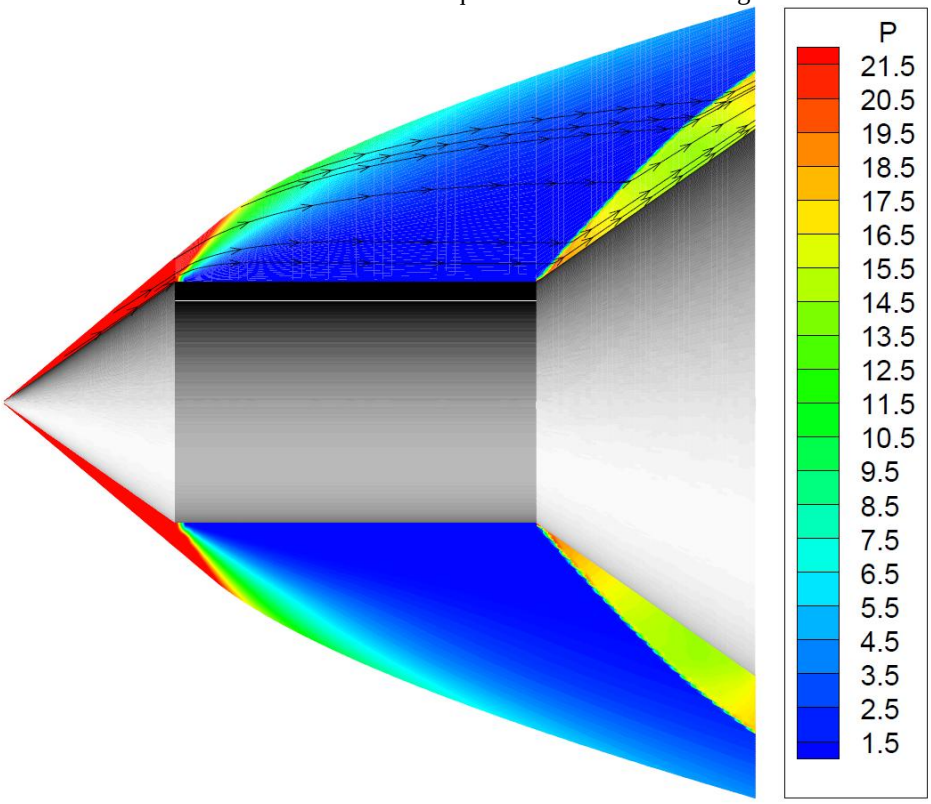

Fig. 4. Visualization of the flow field structure near the cone-cylinder-flare configuration with a nose semiapex angle of $\delta \approx 35°$ and a conical stabilizer semiapex angle of $\theta = 35°$ at a free-stream Mach number of 7

The streamlines are depicted at the top of Fig. 4. The flow pattern and the pressure distribution demonstrate the considered peculiarity of supersonic flow around the conical stabilizer, namely, the nonmonotonic character of the pressure distribution on the flare (see the lower part of Fig. 4).

4. Flow around the cone-cylinder-rear tapering part configuration. The paper presents numerical research of the aerodynamic configuration which consists of the conical nose and conical tail part and the cylindrical part. A case can be considered when the area of the base of the tail part is smaller than the area of the mid-section: the generating line of the tail cone is deflected at a negatively oriented angle.

Results of numerical simulation of aerodynamic loads on the surface of the cone – cylinder – tapering part configuration and a comparison with the results of experimental investigations (Martynov[5]) are presented in Fig.5. The distribution of the pressure coefficient $C_p = \frac{P - P_\infty}{\rho_\infty V_\infty^2 / 2}$ along the length of the cone – cylinder – tapering part configuration with a conical nose semiapex angle of $\delta = 11.5°$ (nose aspect ratio λ=2.46) and a truncated cone semiapex angle of $\theta = -11.5°$ at a free-stream Mach number of 2 is shown. The results of numerical simulation were obtained in the framework of the Euler equations and the Reynolds-averaged Navier-Stokes equations.

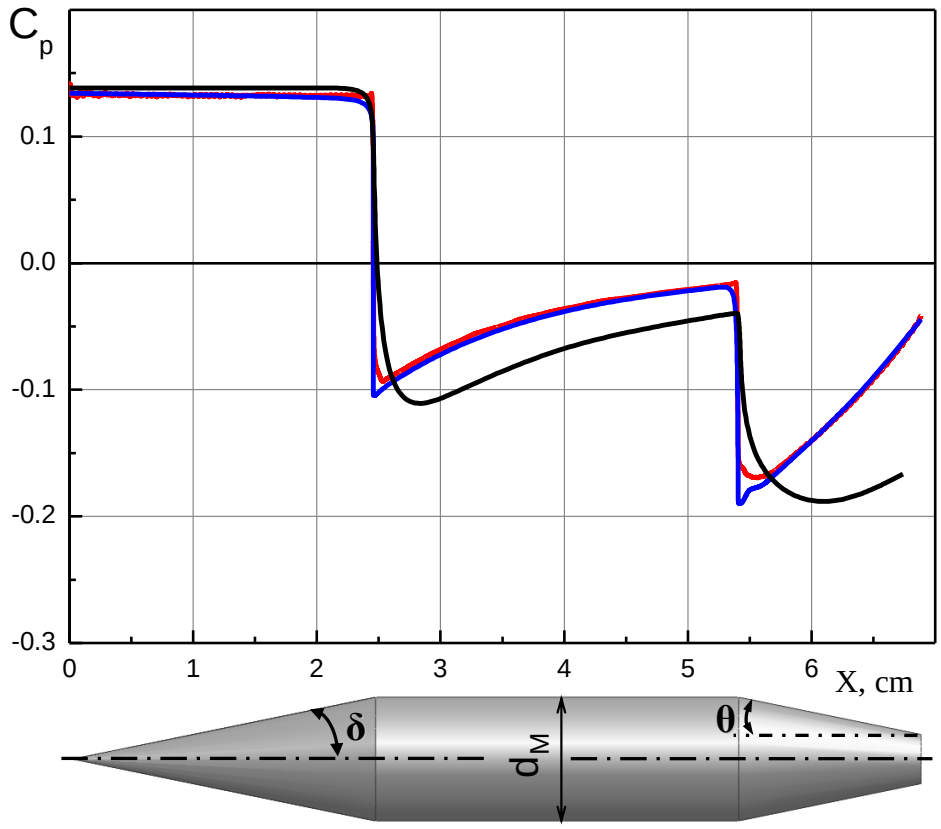

Fig. 5. Pressure distributions C_p on the cone-cylinder-tapering part configuration with a nose semiapex angle of δ =11.5º and a truncated cone semiapex angle of θ = -11.5° at M_∞ = 2: ——— – experiment (Martynov[5]); calculation: ——— – Euler, ——— – Navier-Stokes)

On the cone surface behind the shock attached to the conical nose part the gas pressure remains constant (conical flow condition). According to the calculations the pressure coefficient is C_p = 0.132 (the experimental value is C_p = 0.138).

At the joint of the conical nose and the cylindrical part flow expansion occurs. According to the experimental data on the cylindrical part behind the Prandtl-Meyer expansion the pressure coefficient is C_p = -0.128. According to the inviscid flow results and numerical simulation in the framework of the Navier-Stokes equations the pressure coefficients on the cylindrical part behind the Prandtl-Meyer expansion are C_p =-0.107 and -0.093, respectively.

On the tapering part flow expansion also occurs. In the experiment on the surface of the tapering part behind the Prandtl-Meyer expansion we can see a further decrease of pressure approximately to the middle section of the tail part. The calculation in the framework of the Navier-Stokes equations also indicates a further decrease of pressure behind the Prandtl-Meyer expansion at the joint of the cylinder and the tapering part approximately at the distance of 15% of the length of the tapering part of the model. Up to the tapering part the results of inviscid flow around the considered configuration practically coincide with the numerical simulation results carried out in the framework of the Reynolds averaged Navier-Stokes equations. The calculations carried out in the frame of an ideal gas model indicate monotonic increase of pressure on the whole surface of the rear tapering part (Fig. 5). According to the experimental data from the middle section of the tail part an increase of pressure C_p from -0.2 up to 0.167 happens. The calculation in the framework of the Navier-Stokes equations shows that the pressure begins to increase from the 15% of the length of the tapering part of the model.

The flow field structure in the longitudinal section of the cone – cylinder – tapering part configuration obtained as a result of numerical simulation of supersonic flow in the framework of the Euler and the Navier-Stokes equations is illustrated in Fig. 6. The results of numerical simulation of supersonic flow in the framework of the Reynolds averaged Navier-Stokes equations are presented at the top of Fig. 6. The results obtained in the framework of the Euler equations are depicted at the lower part of the same figure. The flow pattern (distribution of the pressure coefficient P/P_∞) near the considered configuration obtained in the framework of inviscid flow agrees well with the numerical simulation in the framework of the Navier-Stokes equations.

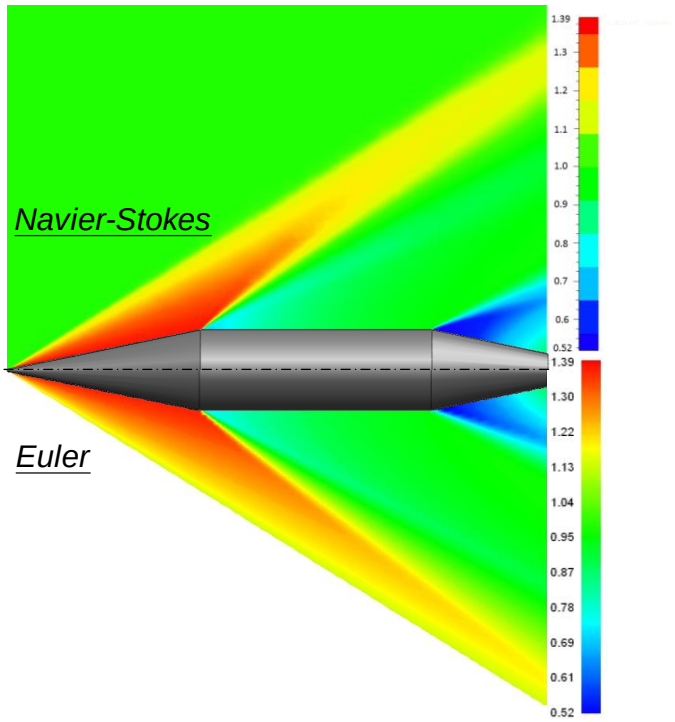

Fig. 6. Visualization of the flow field structure near the cone-cylinder-tapering part configuration with a nose semiapex angle of δ =11.5º and a truncated cone semiapex angle of θ = -11.5° ° at M_∞ = 2

5. Peculiarity of the pressure distribution on the conical tail part. The performed numerical investigations of the aerodynamic configuration with a conical tail part in the form of a truncated cone have shown that the value of the pressure in the aft section highly depends on the nose shape of a flying vehicle. Behind the bow shock attached to the nose we have a high increase of gas pressure, a decrease of the local Mach number and an increase in entropy. The nose conical part with a small aspect ratio (Fig. 4) causes a more considerable entropy change and results in a more emphatic display of the nonmonotonic character of the flare pressure distribution. The results of numerical simulation and the experimental data (Martynov[5]) of flow around the cone – cylinder – tapering part configuration also indicate the nonmonotonic character of the aft section pressure distribution (Fig. 5). The entropy change is determined by the curvature of the shock wave appearing in flow around the nose. The stream passing through the region of the shock located near the nose is characterized by a larger entropy increase than that passing through the conical surface of the shock wave far from the axis of the symmetry of the body. The entropy increase results in a pressure increase, strong vorticity of the flow field, and, correspondingly, a decrease of the local Mach number near the considered configuration. As a result, near the stabilizing surface (flare) of the cone-cylinder-flare configuration with a small nose aspect ratio the surface of the shock wave has a curvilinear form of the generating line (Fig. 4). The entropy change determined by the bow shock wave appearing in flow around the nose results in qualitative and quantitative changes in the pressure distribution on the conical stabilizer (Fig. 3 and 4) as well as on the tapering part (Fig. 5). For the cone-cylinder-flare (see Fig. 3) and the cone – cylinder – tapering part configurations (see Fig. 5) the pressure distribution on the aft section has a nonmonotonic character.

Conclusions. The performed numerical visualization of space flow fields made it possible to establish the key influence of the bow shock wave and the expansion flow interaction on the pressure distribution on the surface of the conical tail part.

Acknowledgements. The work was supported by the Russian Foundation for Basic Research (grant No. 10-01-00208-a).

References

1. Zhilin Yu.L. et al. *On the Binding of Near and Far Fields in the Problem of Sonic Boom. J. Uch. Zap. TsAGI.* 1998, **29**(3-4), p. 111
2. Krasil'shchikov A.P. et al. *Experimental Studies of Bodies of Revolution in Hypersonic Flows*. Fizmatlit, Moscow, 2007
3. Glotov G.F. (2003) *Aerothermodynamics of Flying Vehicles in Photographs*. TsAGI, Zhukovsky, 2003
4. Coleman G.T. *A Study of Hypersonic Boundary Layers over a Family of Axisymmetric Bodies at Zero Incidence.* Preliminary Report and Data Tabulation, Imperial College of Science and Technology. England, I. C. Aero. Rept. 73-06, 1973
5. Martynov A.K. *Applied Aerodynamics.* Mashinostroenie, Moscow, 1972